

**INVESTIGATION OF ZnO NANOSTRUCTURES
ON GLASS SUBSTRATE DEPOSITED BY
THERMAL EVAPORATION METHOD FOR UV
DETECTION**

by

FORAT HAMZAH ABED

**Thesis submitted in fulfillment of the requirements
for the degree of
Doctor of Philosophy**

January 2018

ACKNOWLEDGEMENT

First and foremost, I would like to thank Allah for granting me health and patience to finish this research. I would also like to express my sincere gratitude to my main supervisor, Prof. Dr. Zainuriah Hassan for her valuable guidance and support throughout these study years. Without her comments and continuous encouragement, this dissertation would not have been possible. Thank you professor for having your door open every time I needed help. I would also like to thank my co-supervisor Dr. Naser Mahmoud for his scholarly guidance and support throughout this study.

My appreciation also goes to the staff of the Nano-Optoelectronics Research and Technology Laboratory (N.O.R Lab) and of solid state laboratory for their technical assistance during my laboratory work. My heartfelt gratitude also goes to my family members: to my brother Rafed Hamzah, and wife for their continuous prayers, and endless support when I needed it. Many thanks to all my friends and colleagues who supported and helped me at the School of Physics, Universiti Sains Malaysia.

Forat Hamzah Abed

Penang-Malaysia, January 2018

TABLE OF CONTENTS

ACKNOWLEDGEMENT	ii
TABLE OF CONTENTS	iii
LIST OF TABLES	ix
LIST OF FIGURES	xi
LIST OF SYMBOLS	xvii
LIST OF ABBREVIATIONS	xviii
ABSTRAK	xxi
ABSTRACT	xxiii
CHAPTER 1: INTRODUCTION	1
1.1 Introduction	1
1.2 Motivation and problem statement.....	2
1.3 Research objectives	4
1.4 Research originality	4
1.5 Thesis outline	5
CHAPTER 2: LITERATURE REVIEW AND THEORETICAL BACKGROUND	7
2.1 Introduction	7
2.2 Nanostructures.....	7
2.3 Fundamental properties of ZnO	8
2.3.1 Crystal structures and lattice parameters	9
2.3.2 Optical properties.....	10
2.4 Overview of one-dimensional ZnO synthesis	11
2.5 Overview of three-dimensional ZnO tetrapod synthesis.....	12

2.6	Growth mechanism of ZnO nanostructures	13
2.6.1	Vapor–solid growth mechanism	14
2.6.2	Vapor–liquid–solid growth mechanism	23
2.7	Carrier gas flow	26
2.8	Sputtering system	28
2.8.1	RF sputtering	29
2.8.2	DC sputtering.....	30
2.9	Overview of glancing angle deposition	30
2.10	Laser treatment.....	31
2.11	Overview of ZnO nanostructures based UV detection	32
2.11.1	Theoretical concept of UV detection.....	40
2.11.2	Metal–ZnO–metal contact	42
2.11.3	Operational parameters	44
2.11.3(a)	Sensitivity	44
2.11.3(b)	Responsivity	44
2.11.3(c)	Quantum efficiency	45
2.11.3(d)	Current gain	45
2.11.3(e)	Response and recovery times	46
CHAPTER 3: EXPERIMENTAL AND CHARACTERIZATION TOOLS.....		47
3.1	Introduction.....	47
3.2	Horizontal tube furnace.....	47
3.3	Sputtering system.....	48
3.4	CW CO ₂ laser annealing system	49
3.5	Principles of the characterization tools	50
3.5.1	Structural and morphological tools.....	50

3.5.1(a)	X-ray diffraction (XRD)	50
3.5.1(b)	Field emission scanning electron microscope (FESEM) and energy dispersive X-ray spectrometer (EDX)	52
3.5.1(c)	Atomic force microscopy (AFM)	54
3.5.2	Optical characterization tools	55
3.5.2(a)	Photoluminescence (PL) spectroscopy	55
3.5.2(b)	Ultraviolet-visible (UV-vis) spectroscopy	56
3.5.3	Thin film thickness measurement	57
3.5.4	Photodetection measurement	58
CHAPTER 4: METHODOLOGY		60
4.1	Introduction.....	60
4.2	Substrate cleaning.....	60
4.3	Preparation of ITO seed layer on glass substrate.....	62
4.4	Preparation of Cu and Ag catalyst layers on glass substrate.....	62
4.5	Laser annealing process of seed layer.....	63
4.6	Synthesis condition of catalyst-free 3D ZnO tetrapods	63
4.6.1	Effect of glancing angle deposition	63
4.6.2	Effect of growth temperature.....	64
4.7	Effect of annealing seed layer on ZnO nanowires.....	65
4.8	Effect of intermittently pumped carrier gas on seed/catalyst-free growth of ZnO nanowires.....	66
4.9	Synthesis condition of catalytic growth of 1D ZnO nanorod and nanoneedle arrays on Cu catalyst layer	67
4.9.1	Effect of growth temperature	67
4.9.2	Effect of reaction time.....	67

4.10	Synthesis condition of catalytic growth of 1D ZnO nanoneedles on Ag catalyst layer	68
4.10.1	Effect of Ag film thicknesses	68
4.10.2	Effect of Ar flow rates	68
4.11	Fabrication and measurements of ultraviolet photodetector	70
CHAPTER 5: RESULTS AND DISCUSSIONS: GROWTH AND CHARACTERIZATION OF ZnO NANOSTRUCTURES USING VAPOR-SOLID MECHANISM.....		71
5.1	Introduction	71
5.2	Effect of glancing angle deposition	71
5.2.1	FESEM and EDX characterization	72
5.2.2	Crystalline structure	75
5.2.3	Optical properties.....	77
5.3	Effect of growth temperature.....	81
5.3.1	FESEM and EDX observation.....	81
5.3.2	X-ray diffraction analysis	84
5.3.3	Optical properties.....	85
5.4	Seed/catalyst-free growth of 1D ZnO nanowires with different ITO seed laser annealing	89
5.4.1	Introduction.....	89
5.4.2	Effect of laser treatment on ITO seeds	90
5.4.2(a)	FESEM and AFM observation	90
5.4.2(b)	X-ray diffraction analysis	91
5.4.3	Effect of annealing seed layer on ZnO nanowires.....	93
5.4.3(a)	FESEM and EDX characterization.....	93
5.4.3(b)	Crystalline structure	96
5.4.3(c)	Optical properties.....	98

5.5	Seed/catalyst-free growth of 1D ZnO nanowire balls under an intermittently pumped carrier gas	101
5.5.1	Introduction.....	101
5.5.2	FESEM and EDX observation.....	102
5.5.3	X-ray diffraction analysis	105
5.5.4	Optical properties.....	105
5.6	Summary.....	107
CHAPTER 6: RESULTS AND DISCUSSIONS: GROWTH AND CHARACTERIZATION OF 1D ZnO USING VAPOR-LIQUID-SOLID MECHANISM		109
6.1	Introduction	109
6.2	Catalytic growth of 1D ZnO nanorod and nanoneedle arrays on a Cu catalyst layer	109
6.2.1	FESEM and EDX characterization.....	110
6.2.2	Crystalline structure.....	115
6.2.3	Optical properties.....	117
6.3	Catalytic growth of 1D ZnO nanoneedle arrays on an Ag catalyst layer	122
6.3.1	FESEM and EDX characterization.....	122
6.3.2	Crystalline structure.....	128
6.3.3	Optical properties.....	129
6.4	Summary	132
CHAPTER 7: RESULTS AND DISCUSSIONS: ZnO NANOSTRUCTURES FOR UV DETECTORS.....		133
7.1	Introduction.....	133
7.2	MSM UV PD based on ZnO-Ts coated glass substrate.....	133
7.3	MSM UV PD based on ZnO-NW networks coated glass substrate	140

7.4	MSM UV PD based on ZnO-NW balls under intermittently pumped carrier gas.....	145
7.5	MSM UV PD based on ZnO-NRs coated glass substrate	150
7.6	Summary	155
CHAPTER 8: CONCLUSIONS AND FUTURE WORKS.....		157
8.1	Conclusions.....	157
8.2	Future works	160
REFERENCES.....		161
LIST OF PUBLICATIONS		

LIST OF TABLES

	Page
Table 2.1 Summary of 1D ZnO nanostructures grown by thermal evaporation method via VS mechanism using catalyst-free growth	17
Table 2.2 Summary of 3D ZnO-Ts grown by thermal evaporation method via VS mechanism using catalyst-free growth	20
Table 2.3 Summary of ZnO nanostructures grown via VS mechanism using seed/catalyst free growth.....	22
Table 2.4 Summary of ZnO nanostructures grown via VLS mechanism	26
Table 2.5 Summary of effect of carrier gas on the growth of nanostructures	28
Table 2.6 Summary of fabricating UV PD based on 1D ZnO nanostructures	37
Table 2.7 Summary of fabricating UV PD based on 3D ZnO-Ts nanostructures	38
Table 2.8 Summary of fabricating UV PD based on ZnO nanostructures using glass substrates.....	40
Table 2.9 The electrical nature of ideal metal-semiconductor contacts	43
Table 4.1 Summary of 1D and 3D ZnO nanostructures grown by thermal evaporation method via VS and VLS mechanism.....	69
Table 5.1 Structure properties of ZnO-Ts on glass substrate at a source temperature of 650 °C with various substrate inclined angles	77
Table 5.2 Films thickness, average transmission, and summarize data from PL spectra of ZnO-Ts grown with different substrate inclination angles at a source temperature of 650 °C	80
Table 5.3 Structure properties of ZnO-Ts on glass substrate at a source temperature of 750 °C with various substrate inclined angles	84

Table 5.4	Films thickness, average transmission, and summarize data from PL spectra of ZnO-Ts grown at 750 °C with various substrate inclined angles	87
Table 5.5	Structure properties of ZnO-NWs on ITO seeds as grown and with different seeds annealing temperature	97
Table 5.6	Films thickness, average transmission, and summarize data from PL spectra of ZnO-NW networks on ITO seed layer as grown and with different seed annealing temperatures.....	101
Table 6.1	Structure properties of 1D ZnO-NRs and NNs at different growth temperatures and different growth time.....	117
Table 6.2	Average transmission, films thickness, and summarize data from PL spectra of ZnO-NRs and NNs on Cu catalyst-coated glass substrates.....	120
Table 6.3	Structure properties of ZnO-NNs grown on Ag catalyst layer-coated glass substrates under different Ar flow rates	129
Table 6.4	Average transmission, thickness, and summarize data from PL spectra of ZnO-NNs on Ag catalyst-coated glass substrates.....	131
Table 7.1:	Comparison of the sensitivity, gain, dark current, response time, and recover time of the (Al/ZnO-Ts/Al) MSM structured UV detector on ZnO-Ts at various bias voltages	139
Table 7.2	Comparison of the sensitivity, gain, response time, and recover time of the UV PD based on ZnO-NW networks on ITO seeds/glass	144
Table 7.3	Comparison of the sensitivity, gain, response time, and recover time of the UV PD based on ZnO-NW balls under intermittently pumped carrier gas at various bias voltages	149
Table 7.4	Comparison of the sensitivity, gain, response time, and recover time of the UV PD based on ZnO-NRs on Cu catalyst at various bias voltages.....	154

LIST OF FIGURES

	Page
Figure 2.1	Zinc oxide wurtzite hexagonal structure..... 9
Figure 2.2	Schematic illustration of the growth process for ZnO nanostructures by thermal evaporation method via VS growth mechanism (a) using catalyst-free growth and (b) seed/catalyst-free growth..... 21
Figure 2.3	Schematic illustration of the growth process for 1D nanostructure on Cu catalyst layer by thermal evaporation method via VLS growth mechanism 24
Figure 2.4	RF sputtering setup for physical vapor deposition of thin films..... 29
Figure 2.5	Photoconduction in ZnO nanostructures and energy band diagram (a) under dark condition, and (b) under UV light illumination..... 42
Figure 2.6	A schematic image of an MSM-structured UV photodetectors..... 43
Figure 2.7	Response and recovery times of a typical PD under pulsed light source 46
Figure 3.1	(a) Schematic diagram of the set-up used for the growth of ZnO nanostructures by thermal evaporation, and (b) horizontal tube furnace 48
Figure 3.2	(a) Auto HHV 500 sputtering system, and (b) sample holder containing glass substrates and ITO target..... 48
Figure 3.3	CW CO ₂ laser annealing setup and image of laser system action..... 49
Figure 3.4	Diffraction of an X-ray beam on crystal planes, Bragg's law 51
Figure 3.5	(a) HR-XRD system, and (b) schematic diagram of an X-ray diffraction experiment 52
Figure 3.6	(a) Schematic diagram of field emission scanning electron microscope (FESEM), and (b) photograph of FESEM 53

Figure 3.7	(a) Schematic diagram of atomic force microscopy (AFM), and (b) photograph of AFM	54
Figure 3.8	(a) Schematic diagram of photoluminescence (PL) spectroscopy, and (b) photograph of PL spectroscopy.....	56
Figure 3.9	(a) Schematic diagram of a double-beam UV-vis spectrometer, and (b) photograph of UV-vis spectrometer	57
Figure 3.10	Optical reflectometry system (Filmetrics F20).....	58
Figure 3.11	Schematic diagram of experimental setup for photodetection measurement.....	59
Figure 4.1	Flowchart of the preparation process for 1D and 3D ZnO nanostructures grown on glass substrates by thermal evaporation method using VS and VLS mechanism, and UV PDs.	61
Figure 4.2	Glass slides (Marienfeld Co.) used as substrate	62
Figure 4.3	High-purity Zn powder (99.99%) used as the first source material with the ceramic boat	64
Figure 4.4	Schematic diagram of the set-up used for the growth of ZnO-Ts by thermal evaporation method via VS technique.....	64
Figure 4.5	Schematic diagram of the set-up used for the growth of ZnO-Ts with different growth temperature and inclination angles deposition	65
Figure 4.6	(a) Schematic of the metal shadow used for the fabrication of MSM-structured UV detector, and (b) fabricated ZnO based UV PD	70
Figure 5.1	High and low magnification FESEM images of the ZnO-Ts grown on glass substrates at source temperature of 650 °C with various substrate inclined angles: (a ₁ , a ₂) 0°, (b ₁ , b ₂) 45°, and (c ₁ , c ₂) 90°.	74
Figure 5.2	EDX spectra of the ZnO-Ts grown on glass substrates at a source temperature of 650 °C with various substrate inclined angles	75
Figure 5.3	XRD spectra of grown ZnO-Ts on glass substrates at a source temperature of 650 °C with various substrate inclined angles	76

Figure 5.4	UV–vis transmissions of the ZnO-Ts on glass substrate at a source temperature of 650 °C with various substrate inclined angles. The absorption spectrum is shown in the inset.....	78
Figure 5.5	PL spectra of ZnO-Ts grown on glass substrates at a source temperature of 650 °C with various substrate inclined angles.....	79
Figure 5.6	High and low magnification FESEM images of the ZnO-Ts grown on glass substrates at a source temperature of 750 °C with various substrate inclined angles: (a ₁ , a ₂) 0°, (b ₁ , b ₂) 45°, and (c ₁ , c ₂) 90°	82
Figure 5.7	EDX spectra of the ZnO-Ts grown on glass substrates at a source temperature of 750 °C with various substrate inclined angles	83
Figure 5.8	XRD spectra of grown ZnO-Ts on glass substrates at a source temperature of 750 °C with various substrate inclined angles	85
Figure 5.9	UV–vis transmission of the ZnO-Ts on glass substrate at a source temperature of 750 °C with various substrate inclined angles. The absorption spectrum is shown in the inset.....	86
Figure 5.10	PL spectra of ZnO-Ts grown on glass substrates at a source temperature of 750 °C with various substrate inclined angles.....	87
Figure 5.11	(a)-(d) FESEM images of ITO seeds as grown and with different annealing temperature; (e)-(h) AFM images 3D of ITO seeds.....	91
Figure 5.12	XRD pattern of ITO seed layers deposited on glass substrate, as grown and with different laser annealing temperatures	92
Figure 5.13	The grain sizes and root-mean-square (rms) roughness of ITO seed layers as grown and with different laser annealing temperatures	93
Figure 5.14	High and low magnification FESEM images of ZnO-NW networks on ITO seeds as grown and with different seed laser annealing: (a ₁ , a ₂) as grown, (b ₁ , b ₂) 250 °C, (c ₁ , c ₂) 350 °C, and (d ₁ , d ₂) 450 °C	95

Figure 5.15	EDX spectra of the ZnO-NW networks on ITO seeds as grown and with different seed annealing temperatures.....	96
Figure 5.16	The XRD spectra of ZnO-NW networks on ITO seed-coated glass substrate as grown and with different seed annealing temperatures.	98
Figure 5.17	UV-vis transmission of the ZnO-NW networks on ITO seeds as grown and with different seed annealing temperatures. The absorption spectrum is shown in the inset.....	99
Figure 5.18	PL spectra of ZnO-NW networks grown on ITO seeds-coated glass substrate as grown and with different seed annealing temperatures.....	100
Figure 5.19	High and low magnification of surface and cross-sectional FESEM images of ZnO-NW balls under intermittently pumped carrier gas (a, b, and c); a typical EDX spectrum of ZnO-NW balls (d).....	103
Figure 5.20	Schematic illustration of the growth process for 1D nanostructure via VS growth mechanism under intermittently pumped carrier gas.....	104
Figure 5.21	XRD pattern of ZnO-NW balls grown on glass substrate using VS mechanism under intermittently pumped carrier.....	105
Figure 5.22	UV-vis transmission of the ZnO-NW balls on glass substrate under intermittently pumped carrier. The absorption spectrum is shown in the inset.....	106
Figure 5.23	Room temperature PL spectra of the ZnO-NW balls grown on ITO/glass substrate under intermittently pumped carrier.....	107
Figure 6.1	High and low magnification of surface and cross-sectional FESEM images of the ZnO-NRs and NNs on Cu catalyst at different source temperatures: (a ₁ , a ₂) 450 °C, (b ₁ , b ₂) 550 °C, and (c ₁ , c ₂) 650 °C	111
Figure 6.2	High and low magnification of surface and cross-sectional FESEM images of the ZnO-NRs and NNs on Cu catalyst at different growth time: (a ₁ , a ₂) 30 min, (b ₁ , b ₂) 45 min, and (c ₁ , c ₂) 60 min	114
Figure 6.3	EDX spectrum of the 1D ZnO-NR arrays on Cu catalyst grown at temperature of 450 °C and growth time of 30 min	115

Figure 6.4	XRD patterns of 1D ZnO-NRs and NNs synthesized on Cu catalyst layer: (a) at different growth temperatures (450 °C, 550 °C, and 650 °C), and (b) at different growth time (30, 45, and 60 min).....	116
Figure 6.5	Optical absorption spectra of ZnO-NRs and NNs synthesized on Cu catalyst layer: (a) at different growth temperatures, and (b) at different growth time. The absorption spectrum is shown in the inset	119
Figure 6.6	PL spectra of ZnO-NRs and NNs on Cu catalyst coated glass substrate at different growth temperatures (450 °C, 550 °C, and 650 °C), and (b) at different growth time (30, 45, and 60 min).....	121
Figure 6.7	High and low magnification of FESEM images of the ZnO-NNs grown on different thicknesses of Ag catalyst-coated glass substrate: (a ₁ , a ₂) 10 nm, (b ₁ , b ₂) 20 nm, and (c ₁ , c ₂) 40 nm	124
Figure 6.8	High and low magnification of FESEM images of the ZnO-NNs on Ag catalyst layer under different Ar flow rates: (a ₁ , a ₂) 10 ml/min, (b ₁ , b ₂) 20 ml/min, (c ₁ , c ₂) 30 ml/min, and (d ₁ , d ₂) 40 ml/min.....	126
Figure 6.9	EDX spectra of the ZnO-NNs grown on Ag catalyst layer-coated glass substrates under different Ar flow rates of 10, 20, 30, and 40 ml/min.....	127
Figure 6.10	The XRD spectra of ZnO-NNs grown on Ag catalyst layer-coated glass substrates under different Ar flow rates of 10, 20, 30, and 40 ml/min.....	128
Figure 6.11	UV-vis transmission of the ZnO-NNs on Ag catalyst-coated glass substrates. The absorption spectrum is shown in the inset.....	130
Figure 6.12	PL spectra of ZnO-NNs grown on Ag catalyst-coated glass substrates at different Ar flow rates.....	131
Figure 7.1	Current–voltage characteristics of the ZnO Ts- based UV PDs under dark and UV illumination (365 nm, 1.5 mW/cm ²) at 5 V applied bias	135
Figure 7.2	Room temperature responsivity spectra of the (Al/ZnO-Ts/Al) MSM structured UV detector.....	136

Figure 7.3	The repeatability property (on/off) of the (Al/ZnO-Ts/Al) MSM-structured UV detector under pulsed UV light at various bias voltages.....	138
Figure 7.4	Current–voltage characteristics of the (Al/ZnO-NWs/Al) MSM-structure UV-PD under dark and UV illumination (365 nm, 1.5 mW/cm ²)	141
Figure 7.5	Spectral responsivity of the UV-PDs based on ZnO-NW networks at 5 V reverse bias and under 1.5 mW/cm ² UV illumination.....	142
Figure 7.6	Photoresponse of ZnO-NW networks UV-PD at various bias voltages under pulsed UV light with interval of 20 s.....	143
Figure 7.7	Current–voltage characteristics of the ZnO-NW balls grown on ITO/glass substrate PDs under dark and UV illumination (365 nm, 1.5 mW/cm ²).....	146
Figure 7.8	Spectral responsivity of the UV PD based on ZnO-NW balls at 5 V reverse bias and under 1.5 mW/cm ² UV illuminations	147
Figure 7.9	Photoresponse of ZnO-NW balls UV-PD at various bias voltages under pulsed UV light with interval of 20 s.....	148
Figure 7.10	Current–voltage characteristics of ZnO-NRs based UV detector under dark and UV illumination.....	151
Figure 7.11	Spectral responsivity of the UV PDs based on ZnO-NRs at 5 V reverse bias and under 1.5 mW/cm ² UV illumination.....	152
Figure 7.12	The repeatability property (on/off) of the (Al/ZnO-NRs/Al) MSM-structured UV photodetector under pulsed UV light.....	153

LIST OF SYMBOLS

α	Absorption coefficient
\AA	Angstrom
D	Average grain size
E_g	Band gap energy
θ	Bragg's angle
I	Current
$^{\circ}\text{C}$	Degree Celsius
I_{dark}	Dark current
q	Electric charge
E_{exc}	Excess energy
$h\nu$	Energy of photon
ν	Frequency of incident light
h^+	Hole
d_{hkl}	Inter-planer spacing
P_{in}	Input power of light
d	Interplanar spacing of the crystal planes
l	Liquid droplets
a, b, c	Lattice constant
Φ_m	Metal work function
h, k, l	Miller's indices
O_2^-	Oxygen ion
h	Planck's constant
I_{ph}	Photocurrent
η	Quantum efficiency
Φ_s	Semiconductor work function
ε_{zz}	The strain
β	The full width at half maximum
λ	Wavelength

LIST OF ABBREVIATIONS

AFM	Atomic force microscopy
AC	Alternating current
Al	Aluminum
A	Ampere
Ar	Argon
a.u.	Arbitrary unite
BSE	Backscattered electrons emission
CBD	Chemical bath deposition
CVD	Chemical vapor deposition
CVTD	Chemical vapor transport and deposition
CW	Continuous wave
CO ₂	Carbon dioxide
I-V	Current-voltage
Cu	Copper
CB	Conduction band
DC	Direct current
DLE	Deep level emission
DI	Distilled deionized water
EDX	Energy dispersive X-ray
eV	Electron volt
FESEM	Field emission scanning electron microscopy
FWHM	Full width at half maximum
GLAD	Glancing angle deposition
He	Helium
ITO	Indium tin oxide
In ₂ O ₃	Indium oxide
kV	Kilovolt
LEDs	Light emitting diodes
M	Metal
MSM	Metal–semiconductor–metal
MBE	Molecular beam epitaxial
MOCVD	Metal organic chemical vapor deposition

mW	Milliwatt
mm	Millimeter
ml	Milliliter
mbar	Malabar
NBE	Near band emission
NRs	Nanorods
NNs	Nanoneedles
NWs	Nanowires
N ₂	Nitrogen
nm	Nanometer
O ₂	Oxygen
1D	One dimensional
PL	Photoluminescence
PVD	Physical vapor deposition
PDs	Photodetectors
PLD	Pulsed laser deposition
RF	Radio frequency
R	Responsivity
rms	Root mean square
rpm	Rotations per minute
S	Sensitivity
s	Second
Si	Silicon
SiO ₂	Silicon dioxide
SE	Secondary electron emission
g	The gain
Sn	Tin
SnO ₂	Tin dioxide
Ts	Tetrapods
2D	Two dimensional
3D	Three dimensional
UV	Ultraviolet
UV-vis	UV-visible spectroscopy

V	Volt
VLS	Vapor liquid solid
VS	Vapor solid
VB	Valence band
W	Watt
XRD	X- ray diffraction
0D	Zero dimensional
Zn	Zinc
ZnO	Zinc oxide

**KAJIAN NANOSTRUKTUR ZnO ATAS SUBSTRAT KACA YANG
DIMENDAPKAN OLEH KAEDAH PENYEJATAN HABA UNTUK
PENGESANAN UV**

ABSTRAK

Dalam kerja ini, nanostruktur ZnO dengan morfologi yang berbeza telah difabrikasikan pada substrat kaca kos-efektif menggunakan penyejatan haba mudah dalam relau tiub mendatar konvensional melalui mekanisme wap-pepejal (VS) dan wap-cecair-pepejal (VLS). Kajian ini bertujuan untuk menyediakan satu pendekatan baru untuk sintesis nanostruktur satu-dimensi (1D) dan tiga-dimensi (3D) ZnO menggunakan substrat kos rendah dengan penyejatan haba serbuk Zn dengan kehadiran gas O₂, dan menentukan parameter optimum untuk mengawal kualiti hablur yang tinggi dan sifat optikal, dengan itu meningkatkan prestasi penqesan foto (PDs) ultraungu (UV) berasaskan ZnO yang dihasilkan. Pertama, menggunakan mekanisme VS; pertumbuhan mangkin-bebas ZnO tetrapod 3D (Ts) berjaya dijalankan pada substrat kaca. Sintesis terkawal ZnO-Ts dicapai melalui pemendapan sudut kerling dengan tiga-langkah arah pada substrat kaca dengan sudut kecerunan sebanyak 0°, 45°, dan 90° ke arah aliran gas, dan melalui dua kawasan suhu pertumbuhan: 425-650 °C dan 475-750 °C. Filem nipis ITO yang dipercikkan sebagai lapisan benih substrat kaca bersalut, diikuti dengan suhu penyepuhlindapan benih menggunakan laser gelombang berterusan (CW) CO₂ yang digunakan di sini untuk pertumbuhan benih/mangkin-bebas rangkaian ZnO-NW. Kawalan panjang dan diameter nanodawai disiasat secara sistematik dengan mengubah suhu penyepuhlindapan benih laser pada 250, 350, dan 450 °C. Mekanisme pertumbuhan benih/mangkin-bebas bola ZnO-NW di bawah gas pembawa yang dipamkan secara terputus-putus sebagai kaedah nukleasi yang baru dan mudah disiasat. Keputusan

menunjukkan bahawa kaedah yang dicadangkan memudahkan nukleasi epitaksi dan pertumbuhan ZnO-NW yang berjajar menegak dengan ketumpatan tinggi dengan beberapa mikrometer panjang dan mempunyai diameter yang lebih kecil dan penghabluran yang lebih tinggi berbanding dengan yang difabrikasikan menggunakan pengepaman berterusan tradisional di bawah keadaan pertumbuhan yang sama. Kedua, pertumbuhan bermangkin tatasusunan nanorod (NR) ZnO 1D dan nanojarum (NN) pada substrat kaca bersalut lapisan mangkin Cu dan Ag, masing-masing disiasat melalui mekanisme VLS. Pada mulanya, diameter dan kadar pertumbuhan hablur tunggal ZnO-NRs dan NNs pada substrat kaca bersalut lapisan pemangkin Cu dicapai sebagai fungsi suhu pertumbuhan (450, 550, dan 650 °C) dan tempoh pertumbuhan (30, 45, dan 60 minit) yang berubah. Seterusnya, diameter dan kadar pertumbuhan bermangkin ZnO-NN pada substrat kaca bersalut lapisan mangkin Ag meningkat sebagai fungsi mangkin Ag yang berlainan ketebalan (10, 20, dan 40 nm) dan kadar aliran Ar (10, 20, 30, dan 40 ml / min) pada suhu pertumbuhan yang rendah iaitu 450 °C. Akhirnya, sifat pengesanan foto UV PDs logam-semikonduktor-logam (MSM) telah disiasat berdasarkan yang berikut: pertumbuhan ZnO-Ts 3D/substrat kaca dengan kehadiran persimpangan (persimpangan jarum-dawai); pertumbuhan benih/mangkin-bebas rangkaian dan bola ZnO-NW 1D pada benih ITO/substrat kaca dengan menggunakan pengepaman gas pembawa secara terputus-putus dan pengepaman berterusan tradisional di bawah keadaan pertumbuhan yang sama; dan mengoptimumkan pertumbuhan bermangkin hablur tunggal ZnO-NR pada lapisan mangkin Cu/substrat kaca. Apabila terdedah kepada cahaya 365 nm (1.5 mW/cm^2) pada voltan pincangan 5 V, peranti menunjukkan kepekaan yang tinggi, arus gelap yang rendah, kebolehdeluaran semula yang baik, dan tindak balas dan masa pemulihan yang pantas.

**INVESTIGATION OF ZnO NANOSTRUCTURES ON GLASS SUBSTRATE
DEPOSITED BY THERMAL EVAPORATION METHOD FOR UV
DETECTION**

ABSTRACT

In this work, ZnO nanostructures with different morphologies were fabricated on a cost-effective glass substrate using a simple thermal evaporation in a conventional horizontal tube furnace via vapor–solid (VS) and vapor–liquid–solid (VLS) mechanisms. This study aims to provide a new approach for synthesis of one-dimensional (1D) and three-dimensional (3D) ZnO nanostructures using a low cost substrate by thermal evaporation of Zn powder in the presence of O₂ gas, and determine optimal parameters to control high crystal quality and optical properties, thereby improving the performance of ultraviolet (UV) photodetectors (PDs) based on the produced ZnO. First, using VS mechanism; catalyst-free growth of 3D ZnO tetrapods (Ts) was successfully conducted on glass substrate. Controlled synthesis of ZnO-Ts was achieved through glancing angle deposition by three-step directions of glass substrate with inclination angles of 0°, 45°, and 90° toward the gas flow, and through two growth temperature regions: 425-650 °C and 475-750 °C. Sputtered ITO thin film as a seed layer coated glass substrate, followed by seed annealing temperature using a continuous wave (CW) CO₂ laser, employed here to seed/catalyst-free growth of ZnO-NW networks. The control of the length and diameter of the nanowires were systematically investigated by modifying seed laser annealing temperatures of 250, 350, and 450 °C, respectively. The growth mechanism of seed/catalyst-free ZnO-NW balls under intermittently pumped carrier gas as a new and simple nucleation method was investigated. Results showed that the proposed method facilitates epitaxial nucleation and growth of high-density vertically

aligned ZnO-NWs with several micrometers in length and that have a smaller diameter and higher crystallization compared with those fabricated using traditional continuous pumping under the same growth condition. Second, catalytic growth of 1D ZnO nanorod (NR) and nanoneedle (NN) arrays on a Cu and Ag catalyst layer-coated glass substrate, respectively, were investigated via VLS mechanism. Initially, the diameter and growth rate of high quality ZnO-NRs and NNs on a Cu catalyst layer-coated glass substrate is achieved as a function of varying growth temperature (450, 550, and 650 °C) and growth duration (30, 45, and 60 min). Next, the diameter and growth rate of catalytic growth of ZnO-NNs on a Ag catalyst layer-coated glass substrate increased as a function of different thick Ag catalyst (10, 20, and 40 nm) and Ar flow rate (10, 20, 30, and 40 ml/min) at a low source temperature of 450 °C. Finally, the photodetection properties of the fabricated metal–semiconductor metal (MSM) UV PDs were investigated based on the following: growth of 3D ZnO-Ts/glass substrate in the presence of junctions (needle–wire junctions); seed/catalyst-free growth of 1D ZnO-NWs networks and balls on ITO seed/glass substrate by using intermittently pumped carrier gas and traditional continuous pumping under the same growth conditions; and optimized catalytic growth of high quality ZnO-NRs on the Cu catalyst layer/glass substrate. Upon exposure to 365 nm light (1.5 mW/cm²) at different bias voltages (1, 3, and 5 V), the devices showed high sensitivity, low dark current, good reproducibility, and fast response and recovery times.

CHAPTER 1: INTRODUCTION

1.1 Introduction

Zinc oxide (ZnO) nanostructure is an II–VI compound semiconductor with a direct energy band gap (3.37 eV), a native n-type, and a high exciton binding energy [1, 2]. ZnO have attracted great attention due to its low cost, non-toxic, high thermal stability, high transmittance in the visible region, ease of fabrication and its ability to operate in high temperature and harsh environments [3, 4]. The properties of ZnO is one of the coolest and probably the richest family of nanostructures which pave the way for ZnO nanostructures to occupies a place as a promising material for various future applications. Therefore, ZnO nanostructures have become a great area of investigation because of their improved performance in the field of photonics, electronics and optics which leads to diverse nanotechnological functions [5]. Moreover, the fact that ZnO exhibits the more versatile and abundant configurations of nanostructures with high optical gain of 300 cm^{-1} makes it the material of focus in many applications, especially optoelectronics [6], environmental science [7], actuators and piezoelectric transducers [8], and catalysts [9]. In addition, nanostructured ZnO materials exhibited both piezoelectric and semiconducting properties for fabrication semiconducting piezoelectric coupled devices [10]. ZnO could represent a biocompatible material which can be used in biomedical and biochemical applications [11, 12]. ZnO based UV PDs has attracted great interest in comparison to those fabricated from other semiconductor films [13, 14]. The ZnO based UV detector are effective devices that can be used in a number of applications including environmental monitoring, astronomy, secure chemical/biological analysis, flame sensing and space-to-space communications [15, 16].

ZnO nanostructures are versatile functional materials with various growth sizes and morphologies, such as nanorods [17], nanowires [18], nanobelts [19], nanosheets [20], nanonails [21], nanocombs [22], nanoscrews [23], and tetrapods [24, 25]. Recently, there have been considerable efforts to promote the growth of ZnO nanostructures for optoelectronic applications using different physical and chemical methods, such as chemical bath deposition [26], magnetron sputtering [27], atomic layer deposition [28], spray pyrolysis [29], so-gel method [30], pulsed laser deposition (PLD) [31], and thermal evaporation [32]. Among them, thermal evaporation is considered to be one of the important methods employed to synthesize 1D and 3D ZnO because of its unique features, namely, catalyst-free growth, cost-effectiveness, and easily controlled growth parameters, such as growth rate, distribution on the substrate, and film thickness. In addition, thermal evaporation presents a wide range of nanostructures with various morphologies and with different shapes and sizes [33-36].

1.2 Motivation and problem statement

The controlled synthesis of nanostructures is a promising candidate that plays a vital role in potential applications because the morphological evolution has a significant effect on the performance of functional surfaces by adopting a larger area [34, 36-38]. The large aspect ratio and subwavelength diameter of nanostructures contribute to superior optical properties, such as optical anisotropy, radiative recombination, and surface band bending [39-41]. Moreover, the success in various applications requires the definition and control of the geometry and size of the nanostructures. Consequently, the development and atomic scale tailoring of various physical, chemical and surface properties of nanomaterials are promising to dictate

their interaction in an anticipated manner with wide applications in optoelectronics, sensing electronic, and optics devices [42, 43].

1D ZnO nanostructures like nanorods, nanoneedles, and nanowires have demonstrated potential applications as the next-generation of devices [44, 45], because of its large surface-to-volume ratio, high surface state density, electron confinement properties, and polar nature of the 1D nanostructure [46-48]. However, due to the large surface-to-volume ratio of 1D ZnO nanostructures, surface trap states play a dominant role in the optoelectronic properties of nanoscale devices [49-52]. Consequently, the UV PD based on 1D ZnO has a long response and recovery time because of the oxygen-related hole-trap states at the surface of 1D nanostructures [53-55]. Therefore, many researchers have been focusing on fabricating UV PD based on 1D ZnO with a lot of efforts in order to promote response speed.

On the other hand, 3D ZnO-Ts in different size ranges with several morphologies have been used for various applications as multi-terminal devices; as the diversity in synthesized tetrapods gives the various properties and makes them important for industrial applications. Therefore, ZnO-Ts are of major importance from a technological applications point of view, and thus efficient techniques for growth of different varieties of tetrapod-based networks are demanded [56]. The tetrapods could be designed as multiterminal strain sensors for enhancing sensitivity and response. The UV PD based on ZnO-Ts has a number of advantages over the PD device based on traditional hexagonal ZnO nanostructures due to the sensors based on ZnO-Ts can give multiple responses to a single signal at the same time. In addition, the tetrapods with a natural junction that plays an active role in the building blocks of novel devices because this junction plays a critical role in the

characteristics of ZnO-Ts devices [57-59]. However, relatively few studies have reported on ZnO-Ts nanostructures-based UV PDs due to the difficulty in synthesizing tetrapods and inability to control its morphology and size [60-62].

Consequently, establishing the ability to customize the growth of ZnO nanostructures to produce morphologies, specified surface densities, sizes, and orientation with high crystal quality is necessary in the development of high performance PD devices that possess excellent stability over time, high sensitivity, low dark current, low cost, and exhibit fast response and recovery time.

1.3 Research objectives

The main objectives of this project are:

- 1- To deposit 3D ZnO-Ts on a glass substrate and find a range of variables that can control the growth of tetrapod with different shapes and sizes.
- 2- To investigate high-quality 1D ZnO nanostructures on seed layer and metal catalysts using VS and VLS method, respectively.
- 3- To study the effects of intermittently pumped carrier gas and traditional continuous pumping on the morphology evolution and properties of ZnO nanostructures.
- 4- To improve UV detectors based on ZnO nanostructures grown on a low-cost glass substrate.

1.4 Research originality

The originality of this study includes five key points. Firstly, synthesis of 3D ZnO-Ts on a low-cost glass substrate without using any metal catalysts or seed layer with various morphologies and sizes. Secondly, sputtered ITO thin film as a seed

layer coated glass substrate, followed by seed annealing temperature using a CW CO₂ laser, employed here for the first time to growth of 1D ZnO-NW networks and balls by using VS method. Thirdly, control the growth mechanism of ZnO-NWs balls on ITO seeds-coated glass substrate by thermal evaporation method using intermittently pumped carrier gas as a new and simple nucleation method. Fourthly, growth of high-quality 1D ZnO-NRs and NNs on a Cu and Ag catalyst layer, respectively, coated glass substrate by using VLS method at low temperatures. Finally, enhancing the performance of the fabricated UV PDs based on ZnO nanostructures grown on glass substrate with high sensitivity and fast photoresponse and excellent stability over time.

1.5 Thesis outline

The content of the present study is organized as follows:

Chapter 1 presents a brief introduction of ZnO nanostructures, motivation and problem statement, research objectives, and originality of the current study.

Chapter 2 provides a literature review and background on the fundamental properties of ZnO discusses the growth technology, glancing angle deposition, and laser annealing. This chapter also discusses the growth mechanisms of VLS and VS under intermittently pumped carrier gas and traditional continuous pumping, along with the general principles and theories of MSM–UV detector based on ZnO nanostructures.

Chapter 3 describes the general principles of techniques and equipment used to prepare and characterize ZnO nanostructures.

Chapter 4 discusses the methodology and synthesis processing of seed layer, catalyst layer, and products of 1D and 3D ZnO nanostructures, and the fabrication of UV PDs based on ZnO nanostructures are discussed in Chapter 4.

Chapter 5 illustrates the growth and characteristics of catalyst-free 3D ZnO-Ts through glancing angle deposition at different angles and growth temperatures. This chapter also evaluates the seed/catalyst-free growth of 1D ZnO-NW networks on ITO seeds as grown on glass substrate and with different seed annealing temperatures using CW CO₂ laser annealing system. Chapter 5 also discusses the effects of intermittently pumped carrier gas on the morphological, structural, and optical properties of seed/catalyst-free growth of 1D ZnO-NW balls.

Chapter 6 focuses on the catalytic growth and characterization of 1D ZnO-NR and NN arrays on a Cu catalyst layer-coated glass substrate with varied growth temperatures and durations. This chapter also presents the effects of varying Ag catalyst layer thicknesses and Ar flow rates on the morphology and properties of catalytically grown 1D ZnO-NN arrays on Ag catalyst layer-coated glass substrate.

Chapter 7 shows the fabrication and characterization of MSM UV PDs with catalyst-free grown ZnO-Ts, seed/catalyst-free grown ZnO-NW networks and balls under traditional continuous pumping and under an intermittently pumped carrier gas, respectively, and catalytically grown ZnO-NRs on glass substrates. Chapter 8 presents the conclusions of the study and recommendations for future works.

CHAPTER 2: LITERATURE REVIEW AND THEORETICAL BACKGROUND

2.1 Introduction

In this chapter, the literature review, general principles, and theories of subjects involved in this study are presented. It starts with brief explanation of the fundamental properties, the theories of the synthesis, and the device applications are addressed. The crystal structures, optical properties, and lattice parameters of ZnO nanostructures are reviewed and the 1D and 3D ZnO synthesis are briefly described in this chapter. Discussion the effects of surface morphology, surface trap, surface trap states and oxygen-related hole-trap states at the surface of 1D nanostructure, and thus their effect on the performance of the UV PDs are reviewed. In addition, the major importance of ZnO-Ts in technological applications is described in this chapter. The overview of ZnO growth technology and fundamentals of VS and VLS growth mechanism are also presented. In addition, the review on the DC and RF sputtering, effects of glancing angle deposition and heat treatment by laser annealing temperature are reviewed. The rest of this chapter review the basic theories of MSM–structured UV photodetector and typical mechanism of photoconduction for ZnO nanostructures.

2.2 Nanostructures

Nanotechnology and nanoscience have gained remarkable interest since the last decade and played an important role in improving modern applications due to its unique combination of properties [63]. The materials on a nanoscale-size show a dimension of less than 100 nm according to the dimensions nanomaterials [64, 65].

The nanostructures could be classified into zero-dimensional (0D) (such as quantum dot, and nanoparticle), one-dimensional (1D) (such as nanowires, nanoneedle, nanorod, and nanotube), two-dimensional (2D) (such as nanoflake, nanoleaf, and nanosheet), and three-dimensional (3D) (such as tetrapod, and nanosphere) [66].

Nanostructured materials have attracted much attention because of their unique mechanical, electrical and optical properties that differ from those of their bulk phases. The dimensions and sizes of materials play an important role to determine their properties, where the nanoscale-size of material allows to show greatly changed physical and chemical properties in comparison with same material in the micrometer scale [67-69]. These variations are due to effects that are related to the size of nanostructures and surface state. As the size of nanomaterial decreases, its surface area increases. Increment in the surface area will allow a greater population of its atoms/molecules to be displayed on the surface of nanomaterial rather than its interior [42]. The large length-to-diameter ratio causes an increase in the surface-to-volume ratio. This condition in turn causes an increase in the number of surface atoms. Consequently, the surface atoms bond less with the partial surrounding interior atoms, which leads to change in the properties of the nanostructures [64]. The surface area to volume ratio significantly increases to the level that the material properties are determined by the surface properties. This ratio offers unique characteristics that have extensive applications in various industrial sectors, including medical, electronics, and chemical sectors [70, 71].

2.3 Fundamental properties of ZnO

ZnO is an intrinsically n-type semiconductor with a direct and wide energy band gap with a large exciton binding energy, and it exhibits the most versatile and

abundant configurations of nanostructures. ZnO nanostructures constitute one of the most important functional oxide nanostructures and are advantageous in numerous important practical applications due to their remarkable physical and chemical properties [72]. In this section, the crystal structures and lattice parameters, and optical properties of ZnO nanostructures are presented in detail.

2.3.1 Crystal structures and lattice parameters

The crystal structure of ZnO can simply be described as a number of alternating planes consisting of tetrahedrally coordinated Zn^{2+} and O^{2-} ions which are located on alternatively along the c-axis. ZnO crystallizes in three forms: cubic zincblende, cubic rocksalt, and hexagonal wurtzite [73]. Under traditional condition, the ZnO has wurtzite structure with hexagonal unit cell. Hexagonal wurtzite is the most stable form for ZnO to crystallize and it is characterized by two sub-lattices of O^{2-} and Zn^{2+} ions which form alternating basal planes, where each zinc ion is surrounded tetrahedrally by four oxygen ions and vice versa located on alternatively along the c-axis, as presented in Figure 2.1.

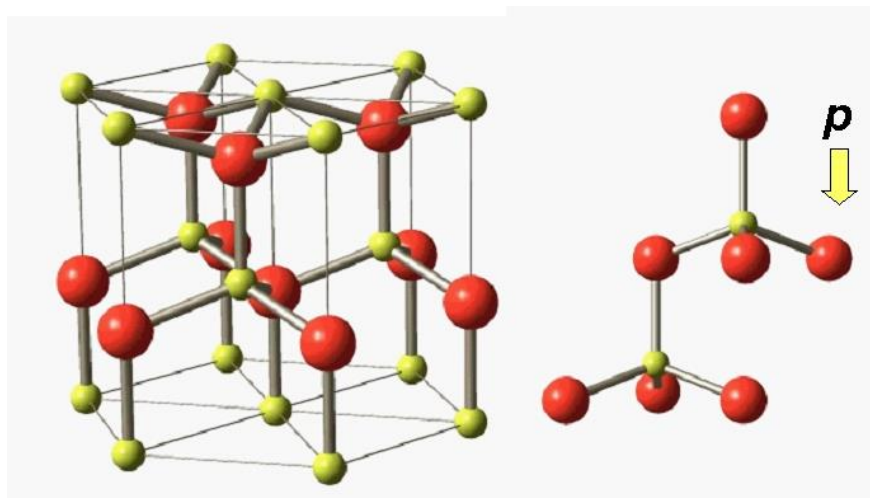


Figure 2.1: Zinc oxide wurtzite hexagonal structure [74].

The wurtzite crystal structure includes a hexagonal unit cell with lattice parameters of a and b lay in the x and y axes. The unit cell in a hexagonal lattice has many lattice plane and direction with their Miller indices. The lattice parameters values of the wurtzite unit cell of ZnO were measured by x-rays diffraction technique [75] to be a and $b= 3.249 \text{ \AA}$, and $c= 5.204 \text{ \AA}$. The ideal axial ratio $c/a= 1.633$, and the density is 5.605 gcm^{-3} , which changes in response to stress or strain [76].

2.3.2 Optical properties

ZnO nanostructures are one of the most important semiconductor material having excellent clarity and superior optical properties [77]. It has direct wide band gap, high exciton energy at room temperature, efficient radiative recombination, and large absorption coefficient at near band edge. The investigations of the optical properties of ZnO nanostructures began in 1960s by Thomas [78], and recently it has potential to become one of the most promising materials among wide-band gap semiconductor materials. The vast majority of the optical transitions of nanostructures have been investigated through photoluminescence (PL) spectra at room temperatures. PL spectra of ZnO mainly consist of a near-band-edge emission (NBE) at the UV region of approximately 380 nm, and a broad deep-level emission (DLE) near the green emission of approximately 485–513 nm. The NBE at the UV region occurs as a result of the recombination of the excitons through an exciton–exciton collision process, whereas the DLE near the green emission occurs as a result of the impurities and native defects [79, 80].

The luminescent properties of nanostructures significantly depend on the perfection of the morphology and content of various defects in the crystal [81-84]. Displacements in the position of the PL peak of ZnO nanostructures with different

sizes and shapes have appeared in PL spectra. The UV emission peak shifts to longer or shorter wavelengths of the PL spectrum due to the surface state effect that has led to change in the energy band gap [85, 86]. Surface states are electronic states found at the surface of materials. They are formed due to the sharp transition from solid material that ends with a surface and are found only at the atom layers closest to the surface. The termination of material with a surface leads to change in the electronic band structure from the bulk material [87]. The electrons in the conduction band (CB) and holes (h^+) in the valence band (VB) are confined spatially by the potential barrier of the surface of nanostructures. Therefore, with the increase of the confinement of electrons and holes led to increase in the optical transition energy from the valence top to the conduction bottom, and the absorption maximum shifts to the shorter wavelength region [85, 88]. In addition, the native defect concentrations in films of ZnO have also been suggested [89, 90]. Several different peaks in visible region that appear in PL spectra of the ZnO nanostructures are ascribed to various defects [34].

2.4 Overview of one-dimensional ZnO synthesis

One-dimensional (1D) semiconductor zinc oxide nanostructures have attracted growing interest for numerous applications and are promising candidates for preparation of advanced devices, because of their large surface-to-volume ratio, electron confinement properties, and polar nature of the 1D nanostructure [1, 91]. In addition, 1D ZnO nanostructures can be useful for electron transport and can decrease the ratio of probability of charge recombination [92]. Recently, the sensors based on 1D ZnO nanostructures attracted a great deal of attention and showed higher sensitivity and improvement capability to detect low concentration gases compared with the other film materials [93, 94]. Moreover, the subwavelength

diameter and large aspect ratio of 1D nanostructure have superior optical and electrical properties such as surface band bending [94], and optical anisotropy [40].

Several methods are used to promote the growth of different shapes of 1D ZnO nanostructures, and they have been synthesized under specific growth conditions at high and low temperatures. High temperatures synthesis includes metal organic chemical vapor (MOCVD), molecular beam epitaxial (MBE), chemical vapor (CVD), and thermal evaporation method, while; low temperature synthesis includes chemical bath deposition (CBD) and electrochemical bath deposition. The growth of 1D ZnO to produce specific sizes, shapes and surface densities has been extensively studied because of their potential technological applications [34, 36], for many applications such photodetectors [95], solar cells [96], light-emitting diodes (LEDs) [97], high volume production of electrodes for batteries [98], photocatalyst [99], as well as their ability to convert mechanical energy into electric power using atomic force microscopy [100].

2.5 Overview of three-dimensional ZnO tetrapod synthesis

ZnO tetrapods (ZnO-Ts) exhibited potential applications, as novel multiterminal devices. The structure of ZnO-Ts is unique, which makes them appear as 3D geometry with four arms pointing along approximately 109.5° angle with each other [101]. The difference between the angles of the arms of tetrapods and its perfect geometry is caused by compensating the stresses generated as a result of dislocations in the core of the seed particles [102]. The arms of tetrapods can sometimes reach up to several micrometers in length, and its hexagonal crystal structure along the c-axis has alternate Zn^{2+} and O^{2-} stacking planes [103]. The junctions of the arms of tetrapods appear in different forms, such as nanorod–

nanowire junction, nanorod–nanoneedle junction, and nanoleaf–nanowire junction [104]. The diversity of synthesized ZnO-Ts, with different size ranges, morphologies, and properties makes them important for various applications. Several reports showed that single ZnO-Ts UV radiation devices and gas sensing have the advantages of low-power consumption, miniaturization, and cost-efficiency [105, 106]. In general, the controlled synthesis of tetrapods with regard to their size and shape has been of significant interest and has led to novel applications that can be investigated depending on their structural properties, which can be controlled through the conditions and parameters that are used in the synthesis of tetrapod nanostructures [107]. Many conditions can have a significant effect on the controlled synthesis of tetrapods using thermal evaporation, such as growth temperature, substrate, gas flow rate, source material, and glancing angle deposition (GLAD).

2.6 Growth mechanism of ZnO nanostructures

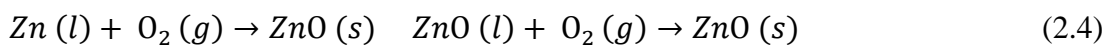
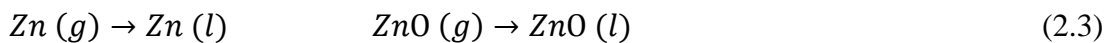
Several physical and chemical methods under specific growth conditions at low and high temperatures are used for growth of ZnO nanostructures. Among these methods, thermal evaporation is one of the physical vapor depositions (PVD) methods that use a conventional furnace, using a horizontal quartz tube. The synthesis of ZnO nanostructures through this method has many advantages compared with other methods, and it is considered to be one of the important methods employed to synthesize ZnO because of its unique features, namely, simple, cost-effectiveness, catalyst-free growth, and easily controlled growth parameters, such as growth rate, distribution on the substrate, and film thickness. In addition, thermal evaporation presents a wide range of nanostructures with various morphologies and with different shapes and sizes [108-110]. Significant research has been conducted on this method to synthesize ZnO with various growth mechanisms. Based on the

condition of the substrate surface; the growth mechanisms of ZnO by thermal evaporation method can be classified into two mechanisms: vapor-solid and vapor-liquid-solid mechanisms.

2.6.1 Vapor–solid growth mechanism

The VS mechanism is a process in which the nucleation and growth of nanostructures occur on the substrate surface without using a metal catalyst [111]. This mechanism includes two techniques, namely, catalyst-free growth and seed/catalyst-free growth. In general, the growth of ZnO nanostructures through thermal evaporation by the VS mechanism can be divided into two steps: nucleation and growth. Nucleation is an agglomeration process of molecules that forms the first grain of the nanostructure [112-115].

Constantly heating the reaction zone inside the horizontal tube under gas flow causes the Zn vapor to react with O₂ gas to form the nucleus of the ZnO. The Zn or ZnO vapor will condense into liquid droplets of Zn (*l*) or ZnO (*l*) located on the substrate. The forming mechanism of the ZnO nanostructures can be summarized by the following relations [116, 117].



The liquid droplets (*l*) of ZnO are condensed or deposited on the surface of substrate by carrier gas flow. The liquid droplets represent the initial stage of

nucleation process of the nanostructure, which acts to create favored nucleation sites on the substrate. The nucleation sites absorb the vapor phase until supersaturation is reached, and the growth of the nanostructure begins from these sites [72, 118].

The VS mechanism can be classified into two growth methods as a result of the surface condition of the substrate: catalyst-free growth and seed/catalyst-free growth. In the VS mechanism using catalyst-free growth, the nucleation and growth of nanostructures directly occur on the substrate surface without using metal catalyst or seed layer [Figure 2.2 (a)]. The substrate should possess important features for the growth of nanostructures and must be stable at the growth temperature specified; significant parameters to be considered include surface morphology, structure, and lattice mismatch with the nanostructure [72, 119].

Several studies have been conducted to synthesise 1D ZnO nanostructures by VS mechanism using catalyst-free growth. For example, Umar et al. [118] reported on the growth of ZnO-NWs on Si(100) substrates following VS mechanism without using metal catalysts, seed layer, or additives with diameters in the range of 60–100 nm and lengths of 5 μm . Before starting the reaction, the substrate was pretreated under nitrogen and hydrogen environment for 20 min at 500 $^{\circ}\text{C}$ and after loading the sample, the chamber pressure was reduced to 2 Torr using a rotary vacuum pump. The oxygen and nitrogen gases were introduced into the reaction chamber with 2:1 flow rates respectively, after the pretreatment step. The growth process was carried out by thermal evaporation of Zn powder in a horizontal quartz tube furnace at 550 $^{\circ}\text{C}$ –650 $^{\circ}\text{C}$ for 1hr. Suh et al. [120] synthesized catalyst-free growth of ZnO nanostructures on Si substrate without the use of any catalyst or additives by thermal evaporation of high-purity metallic Zn powder in the presence of O_2 gas in a horizontal tube furnace system, which consists of two zones. The source material

placed in the temperature ranged between 515 and 580 °C, while the Si substrates were placed into three different temperature zones: 470–515 °C, 555–580 °C, and 515–555 °C for 1.5 hr; with increasing distance between substrate, source material, and substrate temperature; the formation of ZnO nanostructures changed from nanosheets to microflowers and then nanowires. Ouyang et al. [121] reported a catalyst-free synthesis of macro-scale 1D ZnO nanonails on Si (100) substrate using VS method without any catalyst or seed layer through simple thermal evaporation of about 0.1 g Zn powder in the presence of O₂ gas by a horizontal tube furnace system; vertically aligned nanonails with a side length of 1.4 μm were grown as the source temperature was gradually increased from room temperature to 700 °C at a rate of 25 °C/min for 90 min. Liu et al. [122] reported on the growth of catalyst-free ZnO-NWs on Si substrate by a simple thermal evaporation of pure Zn powders under air ambient in a horizontal quartz tube using VS mechanism without any seed or catalyst; the furnace was heated to 750 °C for 120 min under a constant flow of pure O₂ gas, with the flow rate of 2 ml/min. The diameter of the nanowires was 40-100 nm, and the length was about several micrometers and some aligned ZnO-NWs with smooth surface were also detected. Lee et al. [123] reported on ZnO-NWs that were synthesized by thermal evaporation of ZnBr₂ powder in a horizontal tube furnace under air atmosphere at relatively low temperatures of 600–900°C with a heating rate of 10°C/min. Any catalysts and seed layers were not used in the synthesis of nanowires. The ZnBr₂ powder was evaporated and reacted with O₂ gas in air for 1h of oxidation process. Nanowires were observed with the lower density at a low temperature of 600°C and increasing the temperature to 700°C; needle-like structures with high density were observed with a typical diameter of 100 nm and lengths up to several micrometers. Pushkariov et al. [124] fabricated vertical-aligned ZnO-NR arrays on Si substrate using catalyst free thermal vapor deposition using a horizontal

tube furnace with a small quartz tube opened on both sides at quite low temperatures of 550°C–600°C for 30 min. The growth process was carried out by simple thermal evaporation of metallic granule Zn in Ar and O₂ gas mixture, transferring vapor precursors to substrate and subsequent deposition of ZnO-NRs on the substrate from the vapor phase without the use of any catalysts or seed layers. Average diameter of the rods is about 50 nm and the average height of rods increases with the increasing substrate-to-source distance from 200 nm to 800 nm. Table 2.1 summarizes the various types of 1D ZnO nanostructures grown by thermal evaporation method via VS mechanism using catalyst-free growth.

Table 2.1: Summary of 1D ZnO nanostructures grown by thermal evaporation method via VS mechanism using catalyst-free growth

Method	Crystal Structures	Sub.	Source Temp. (°C)	Growth Time (min)	Ref.
VS mechanism-catalyst-free	ZnO-NWs	Si(100)	550–650	60	[118]
VS mechanism-catalyst-free	Nanosheets to microflowers and then nanowires	Si	515–580	90	[120]
VS mechanism-catalyst-free	ZnO nanonails	Si(100)	700	90	[121]
VS mechanism-catalyst-free	ZnO-NWs	Si	750	120	[122]
VS mechanism-catalyst-free	ZnO-NWs	Si	600–900	90	[123]
VS mechanism-catalyst-free	ZnO-NR arrays	Si	550–600	30	[124]

On the other hand, for the growth mechanism of 3D ZnO-Ts via a VS mechanism, a consensus exists in the literature, suggesting that the nanoarms grow after the nucleation of a core structure [125]. The ZnO nuclei that form in the atmosphere are octahedral nuclei [126], which are consistent with the octa-twin

nucleus model [127], and highlight the synthesis morphology of ZnO-Ts. According to the principle of the lowest surface energy, the octahedral nuclei induce the formation of ZnO-Ts. In addition, the arms of the tetrapod has a preferential growth direction along the c-axis orientation, which is faster than in any other direction [128].

Recently, many efforts have been devoted to grow 3D ZnO-Ts by VS mechanism using catalyst-free growth. For example, Ronning al. [129] reported on ZnO-Ts on Si (100) substrate through thermal evaporation of metallic Zn under ambient conditions in the presence of O₂ gas in a tube furnace. The furnace was heated up to 1100 °C using a ramp of 5 °C/min for 30 min; the arms of tetrapods strongly depend on the growth temperature, in which the length varies from 300 nm to 1.5 μm with leg diameters of about 30 to 650 nm with the increasing temperature. Chen et al. [104] reported the growth of tetrapod ZnO nanostructures on Si substrate with different morphologies of rod–wire junction, dumbbell-like and cone-like by vapor phase oxidation from Zn powder using purity O₂ with Ar as the carrier gas in Alumina crucible at different growth temperatures. The large-scale of ZnO-Ts with nanorod–nanowire type structures were obtained at 900 °C for 60 min; the rods have a length of about 1–2 μm, and their diameter is not uniform, decreasing from 180 nm (the root section) to 80 nm (the end section). Delaunay et al. [130] reported a fabricated ZnO-Ts network directly onto a quartz substrate by thermal oxidation reaction in air from Zn powder which was placed in a quartz tube and heated at 900 °C for 30 min. The morphologies were found to depend on the content of water in air, the network of tetrapods was obtained with a small content of water vapor that formed a highly porous layer with a high surface to volume ratio; the arms of tetrapods possess several micrometres and diameters in length in the 0.1–1 μm range.

Newton et al. [24] prepared ZnO-Ts onto bare Si substrate via chemical vapor transport and deposition (CVTD) without using any metal or seed layer by thermal evaporation of a mixture of zinc carbonate powder and graphite powder in a horizontal quartz tube furnace using two zones in this region of the furnace at 900 °C and 600 °C for the source material and substrate, respectively. The synthesized tetrapods with arm lengths of 200 nm to 10 µm and cross-sectional widths of 50 nm to 500 nm were achieved as a function of source material containing a mixture.

Nguyen et al. [131] fabricated ZnO-Ts nanostructures on Si substrates without a catalyst or seed layer through thermal evaporation of Zn powder in a horizontal quartz tube furnace in the presence of O₂ gas using the VS process at 700 °C–950 °C for 60 min. The Zn powder was placed at the sealed end of the quartz tube while the Si substrate was placed in the centrum of the furnace. The tetrapods appeared when the evaporation temperatures were at 700 °C and 800 °C; at 700 °C, the tetrapods started to form but the lengths were short, while at 800 °C, the length was longer at about 200 nm.

Mustonen et al. [132] reported on the growth of ZnO-Ts on PET substrate by the growth reactor which consists of a vertical quartz tube that is inserted into the furnace and flow reactor by gas phase oxidation of Zn vapor in an air atmosphere. Morphology of the product was varied from spherical nanoparticles to ZnO-Ts. The morphology of ZnO-Ts was modified by pressure of Zn vapor by changing the evaporation temperature in the reactor zone; the highest aspect ratio of tetrapods structure was obtained at 700 °C for 30 min with length up to 0.5 µm and diameter of 10-20 nm.

Hassan al. [111] prepared ZnO-Ts on Si (100) substrate without using a metal catalyst through thermal evaporation of Zn powder in a horizontal quartz tube furnace in the presence O₂ gas using VS process in a horizontal tube furnace system. The morphological and optical properties of ZnO-Ts were strongly influenced by changes in reaction durations; the tetrapods appeared

upon extending the reaction time to 60 min at 900 °C with the length of legs ranging from 4 to 7 μm and average diameters of 1 μm , and the length of the legs was 7 μm with a diameter of 1.2 μm . Table 2.2 summarizes of 3D ZnO nanostructures grown by thermal evaporation method via VS mechanism using catalyst-free growth.

Table 2.2: Summary of 3D ZnO-Ts grown by thermal evaporation method via VS mechanism using catalyst-free growth

Method	Crystal Structures	Sub.	Source Temp. (°C)	Growth Time (min)	Ref.
VS mechanism-catalyst-free	ZnO-Ts	Si (100)	1100	30	[129]
VS mechanism-catalyst-free	ZnO-Ts	Si	900	60	[104]
VS mechanism-catalyst-free	ZnO-Ts network	Quartz	900	30	[130]
VS mechanism-catalyst-free	ZnO-Ts	Si	900 and 600	–	[24]
VS mechanism-catalyst-free	ZnO-Ts	Si	700–950	60	[128]
VS mechanism-catalyst-free	ZnO-Ts	PET	700	30	[132]
VS mechanism-catalyst-free	ZnO-Ts	Si (100)	900	60	[111]

On the contrary, in the VS mechanism using seed/catalyst-free growth, the nucleation and growth process of nanostructures occurred on the seed layer surface [Figure 2.2 (b)] [133, 134]. In this case, the seed layer plays an important role in facilitating the growth of nanostructures [135, 136]. The liquid droplets that represent the initial stage of nucleation process create favored nucleation sites on the seed surface. The nucleation sites absorb the vapor phase until supersaturation is reached, and the growth of the nanostructure begins from these sites. Therefore, the seed layer is highly important in enhancing the nucleation of the ZnO growth. Consequently,

the relationship between the nanostructure and the seed layer should be understood because the properties of the ZnO mainly dependent on the properties of the seed layer, such as morphology, grain size, roughness, and crystalline density. Therefore, preparing a high-quality seed layer is a significant step towards promoting the growth of ZnO nanostructures, which can help promote the development of potential applications and novel devices [137, 138].

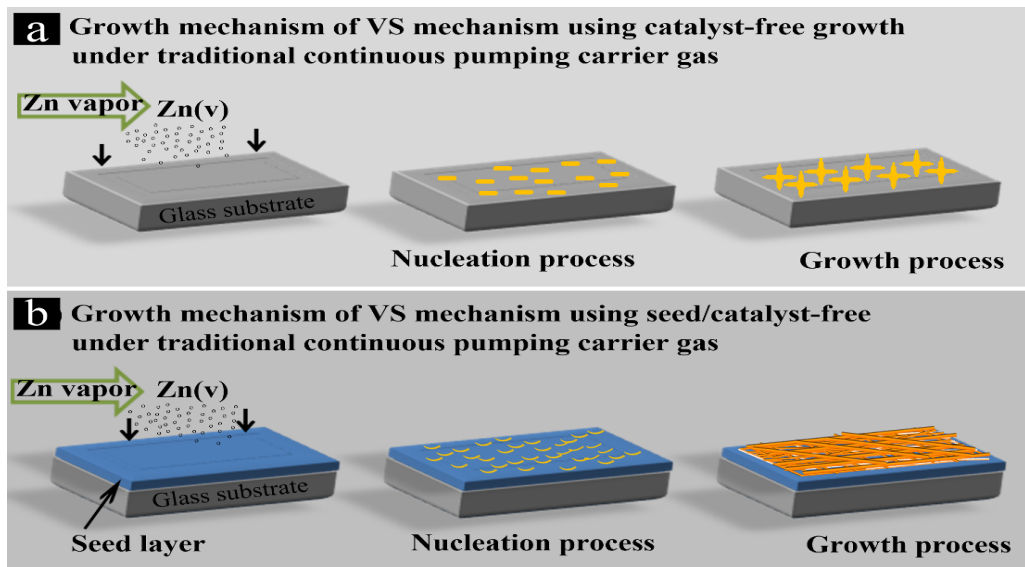


Figure 2.2: Schematic illustration of the growth process for ZnO nanostructures by thermal evaporation method via VS growth mechanism (a) using catalyst-free growth, and (b) seed/catalyst-free growth [139].

Several studies have investigated ZnO nanostructures growth through VS mechanism using the seed/catalyst-free growth. For example, Ahmad et al. [140] fabricated seed/catalyst-free growth of ZnO-NRs and nanostructures by thermal evaporation of Zn powder in the presence of O_2 gas in dual zone furnace at temperatures of 600°C, 800°C, and 1,000°C, respectively, on single-layer graphene and multilayer graphene-coated Si substrates; the morphological and optical properties of ZnO nanostructures were influenced by changes in substrate position and graphene thickness. Aziz et al. [141] synthesized seed/catalyst-free growth of

ZnO-NRs through thermal evaporation of Zn in the presence of O₂ gas on single-layer graphene-coated (SiO₂)/Si substrate; high-density, vertically aligned ZnO-NRs with different morphologies and quality levels were grown at different source temperatures of 600 °C and 1,000 °C. Rusli et al. [142] performed seed/catalyst-free growth of ZnO-NRs and nanoclusters on multilayer graphene-coated SiO₂/Si substrate inclined at 45° in the second zone by using thermal evaporation in dual zone furnace at 600 °C, 800 °C, and 1,000 °C, respectively; the effects of substrate temperatures on the morphology and optical properties of ZnO nanostructures were then investigated. Table 2.3 summarizes of ZnO nanostructures grown by thermal evaporation method via VS mechanism using seed/catalyst-free growth.

Table 2.3: Summary of ZnO nanostructures grown via VS mechanism using seed/catalyst free growth

Method	Sub.	Seed Layer	Crystal Structures	Source Temp. (°C)	Growth Time (min)	Ref.
Thermal évaporation method using VS-seed/catalyst-free	SiO ₂ /Si	Single-layer grapheme and multilayer graphene	ZnO nanostructures, ZnO cluster structures, and ZnO-NRs	1,000	60	[140]
Electrochemical deposition method using VS-seed/catalyst-free	SiO ₂ /Si	Single-layer graphene	Nanorod clusters, nanoporous-like morphological structures, and vertical nanorods	80	60	[138]
Thermal evaporation method using VS-seed/catalyst-free	SiO ₂ /Si	Multilayer graphene	Nanoclusters, nanorods, and thin films	1,000	60	[142]

2.6.2 Vapor–liquid–solid growth mechanism

VLS growth mechanism is an important approach for growing uniform and aligned 1D nanostructure. In this method, catalyst layer should be deposited as metal coating on the substrate surface to grow ZnO nanostructures. The most commonly used metal catalysts are Au, Ag, and Cu [143-145]. Metal catalysts exert a significant effect during the synthesis process of nanostructures because of the altered lattice constant of the catalyst layer [146]. The nucleation and growth process of ZnO via a VLS mechanism occurs as a result of the combination of vapor deposition with catalyst particles to form liquid alloy droplets on the substrate [147-150]. Consequently, the catalyst particles–Zn alloy process reaches certain solubility depending on the temperature; then, the Zn vapor begins to precipitate out at the interface between the surface and droplet [151-154]. The growth of nanostructures through direct adsorption of a gas phase on a solid surface (VS mechanism) is generally very slow; VLS growth mechanism exceed this slowness through introducing a catalytic liquid alloy phase which can quickly adsorb vapor to saturation level, thereby causing a growth of nanostructures from the nucleation sites of the liquid–solid interface [155-157]. This method can be divided into three stages, as follows: first, the Zn vapor and metal catalysts form liquid alloy droplets during the heating process at a certain temperature, representing the initial stage of nucleation process. Second, crystal nucleation occurs upon gaseous species adsorption until supersaturation is reached, and the formed sites serve as nucleation sites on the substrate. Finally, the axial growth of the nanostructures begins from these sites [119, 158]. Figure 2.3 shows a schematic illustration of the growth process for 1D nanostructure via VLS method.

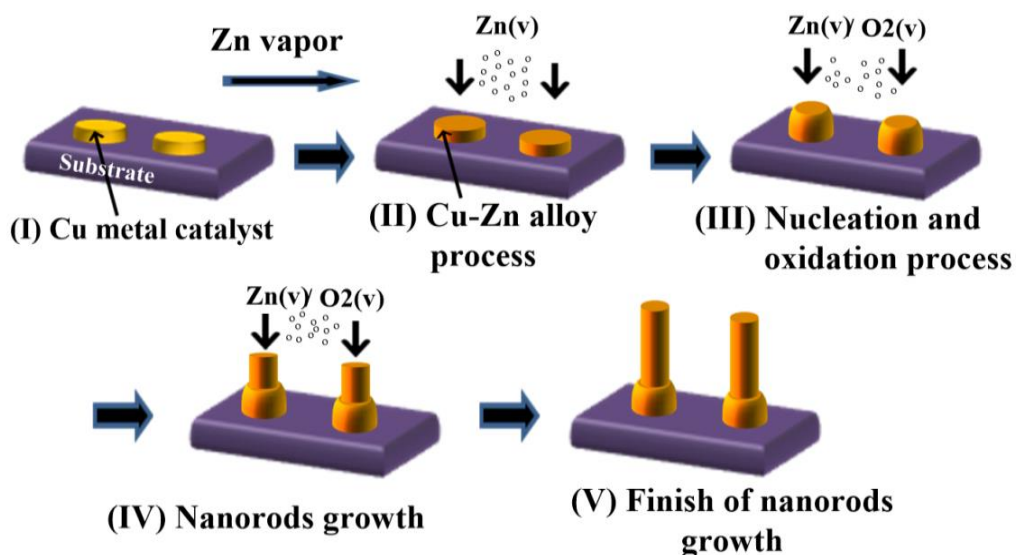


Figure 2.3: Schematic illustration of the growth process for 1D nanostructure on Cu catalyst layer by thermal evaporation method via VLS growth mechanism [119].

The VLS mechanism was proposed for the first time in 1964 by Ellis and Wagner for the epitaxial deposition of silicon whiskers on Au as a metal catalyst [159]. The thermal evaporation of a mixture of ZnO powder with Au nanoparticle, graphite, and Se with Zn powder to obtain 1D ZnO nanostructures were used in 2001 by Huang et al [160], and Yao et al [161]. In 2002, Gao and Wang proposed the use of Sn as an effective catalyst layer for growing 1D ZnO nanostructures by thermal evaporation of the mixture of ZnO and SnO₂ powders at 1300 °C for 1 h under pressure of 300-400 Torr and Ar carrier gas flow rate of 50 sccm through a VLS growth method [162]. Wei, et al. [163] reported single-crystal ZnO-NWs grown onto a glass substrate using self-seeded VLS mechanism via ultrasonic spray-assisted CVD at a temperature slightly below the melting point (420 °C) of Zn, in which liquid Zn droplets coated glass substrate were used as a catalyst layer. Recently, researchers have focused on fabrication ZnO nanostructures through VLS method by